PCCP

Accepted Manuscript

ROYAL SOCIETY OF CHEMISTRY

www.rsc.org/pccp

Physical Chemistry Chemical Physics
CREATED USING THE RSC LaTeX PCCP ARTICLE TEMPLATE – SEE www.rsc.org/electronicfiles FOR DETAILS
ARTICLE TYPE www. rsc.org/xxxxxx | XXXXXXXX

Polymorphic MnAs nanowires of magnetic shape memory alloy†

C. Echeverría-Arrondo,*[ac] J. Pérez-Conde,[b] and A. Ayuela[dc]

Received Xth XXXXXXXXXX 20XX, Accepted Xth XXXXXXXXX 20XX
First published on the web Xth XXXXXXXXXX 200X
DOI: 10.1039/b000000x

We describe a magnetic shape memory alloy, in which it is the nanostructural confinement that influences both the crystal geometry and the electronic and magnetic properties. We use calculations from first-principles on shape memory MnAs nanowires to study the influence of strain on the resulting crystallographic phases, which arise at their surfaces. We show that MnAs nanowires as thin as two nanometers can be stable in a new crystal geometry which is induced by one-dimensionality and hence is unknown in the bulk, typically hexagonal. The changes between phases caused by differences in strain require the existence of twin domains. Our analysis suggests that the strain-induced structural transition -that is here described for MnAs compounds- could be applied to other (magnetic) shape memory nanowire systems for applications in a range of devices from the mechanical to the magneto-electronic.

1 INTRODUCTION

Nanocrystalline structures such as quantum wires are attractive because of their particular properties that arise from low dimensionality and quantum confinement which make them of interest in the design of new nanodevices.[1–5] These nanocontacts, when synthesised from semiconductors such as Si,[6] CdS[7] in group II-VI, and GaN[8] in group III-V, show considerable promise in nanoelectronics. Ferromagnetic nanowires fabricated using the traditional materials Co, Fe and Ni[9–11] and some alloys such as MnAs[12] may well be of some use in ultra-high density recording devices[11,13] and in nanomagnetism. In the field of study that lies between semiconductor electronics and magnetism, one-dimensional nanostructures made of magnetic materials add to the set of interesting functionalities of spintronics. Wires that are made entirely of diluted magnetic semiconductor GaAs:Mn have already been grown.[14] At epitaxial semiconductor-magnet interfaces, semiconductor wires have magnetic dots of shape memory alloy MnAs[15] attached to them, or they are fully covered with MnAs wires around cores of III-V semiconductor GaAs.[16] Ferromagnetic nanowires made of MnAs are also fabricated on GaAs surfaces using lithographic[12] and epitaxial[17] techniques. In all cases, the resulting MnAs/GaAs heterojunctions are clean, atomically sharp, and thermodynamically stable.[18,19] In these hybrid systems, magnetic shape memory alloys such as MnAs are easily grown on semiconductor surfaces due to their commensurability at the interface. Shape memory nanostructures made of MnAs can be subject to considerable strain because of confinement, and in the same way the application of strain will induce changes in other properties, as previously found in semiconductor nanocrystals.[20] The theoretical study of nanowires made of magnetic shape memory alloys is therefore necessary. We focus on MnAs as a prototype material. In nanowires, its major advantage as compared with nonmagnetic shape memory alloys, such as CuAlNi, is the spin-polarized electronic structure which further depends on the crystal phase, of interest to nanomagnetism and spintronics. Furthermore, such wires are expected to change their magnetic properties by mechanical loading, what could be beneficial for sensors.

Magnetic shape memory alloys may be grown relatively easily on semiconductor surfaces due to the softness of their phase transitions, which involve several crystal structures. This softness comes from the reversible transformation between a high-temperature phase (known as austenite) and a low-temperature phase (martensite).[21] Recent experimental work has shown that the two phases are involved in the nonmagnetic shape memory ternary alloy CuAlNi and are more stable in nanoscale pillars than they are in the bulk.[22] In the case of the magnetic shape memory alloy MnAs, the high-temperature and less-ordered orthorhombic phase changes at low temperatures to an hexagonal NiAs-type ferromagnetic phase.[23] The two structures are related by a shear of the atomic lattice, together with a relaxation of the atoms in the unit cell. Above 318 K, the hexagonal symmetry is transformed into the orthorhombic MnP-type, and the ferromagnetic order of the Mn spins changes to antiferromag-

[a] *Department of Physical Chemistry, Basque Country University UPV/EHU, 48080 Bilbao, Spain; E-mail: echeverria.arrondo@gmail.com*
[b] *Department of Physics, Public University of Navarre, 31006, Pamplona, Spain*
[c] *Donostia International Physics Center (DIPC), 20018, San Sebastián/Donostia, Spain*
[d] *Materials Physics Center CFM-MPC Centro Mixto CSIC-UPV/EHU, Department of Materials Physics, 20018, San Sebastián/Donostia, Spain*

netic, with a random distribution of spin-up and spin-down Mn planes.[24] This hexagonal-to-orthorhombic transformation yields a shape-memory effect in MnAs.[23] Although zinc-blende MnAs is unstable in the bulk, it has been successfully grown in the form of quantum dots[25] and thin films.[26] In the present context of magnetic nanowires of shape memory MnAs, we herein address the important question of the stability of the crystal phases under confinement, and how the crystal structure affects their electronic and magnetic properties.

We herein discuss our investigation of polymorphic MnAs shape memory nanowires using density functional theory. In particular, we address the geometrical stability of hexagonal NiAs-type and zinc-blende crystal structures. Surprisingly, the most stable one is neither the hexagonal nor the zinc blende, but a different phase induced by the low dimensionality of the MnAs nanowires. This ground-state structure is characterized by eight nearest neighbors around the high-symmetry central column of Mn atoms, and it is orthorhombic far from the surface. This new geometry is hereafter referred to as "8-index". The fact that the crystal ground state is neither hexagonal nor zinc-blende is unexpected, and illustrates the way in which strain plays an important role in the stabilization of one-dimensional crystalline semiconductors. In order to understand this confinement-induced behavior, we analyze strain in ferromagnetic MnAs nanowires using their associated winding numbers,[27] and show that MnAs nanowires cannot be *continuously* deformed from the 8-index phase into zinc-blende due to different winding numbers. The formation of either dislocations or twins in the zinc-blende phase under strain therefore justifies the consideration of a different energetic order. In addition, we show that ferromagnetic MnAs nanowires are metallic in the 8-index phase, with large carrier velocities at the Fermi energy, while the hexagonal and cubic phases are half-metallic. The size of the nanowires is crucial for their properties: For larger wires, it is expected to recover the bulk behavior of MnAs magnetic shape memory alloy, as confinement effects gradually disappear.

2 THEORETICAL AND COMPUTATIONAL DETAILS

We start our investigation of the threefold polymorphism of ferromagnetic MnAs nanowires by relaxing two bulk-like input geometries, namely hexagonal and zinc-blende, as depicted in Fig. 1. We build our nanowires from the experimental MnAs structures obtained in bulk and thin films, hexagonal and zinc blende, well known up to date. The MnAs wires are then stretched or compressed. Small pseudohydrogens[28] are included in order to avoid surface effects and mimic the surrounding environment. We calculate their geometrical, electronic, and magnetic properties using the projector augmented-wave method, as implemented in VASP (Vienna Ab-initio Simulation Package).[29,30] We use the GGA+U exchange-correlation approach[31] to model the strong interactions between the Mn 3d electrons through the U Coulomb and J exchange parameters, $U = 4$ eV and $J = 0.8$ eV.[32] The accuracy and transferability of our values for U and J have been thoroughly tested, not only in other structures with MnAs bonds, such as (Ga,Mn)As and (In,Mn)As,[32–34] but also in other materials, e.g. MnN and (Ga,Mn)N.[35] Furthermore, our calculations with and without U produce the so called 8-index phase as most stable phase, given in Fig 1 (c). Our results are thus stable relative to the variation of U and J parameters. This finding is not puzzling in view of other authors' results for Mn atoms in different wires also found U-independent.[36] Other parameters are fixed as in our previous works for Mn-doped nanocrystals.[37–39] The atomic positions are relaxed until the forces on the atoms are smaller than 0.02 eV/Å. We take six k points in the Γ-X region of the first Brillouin zone to calculate relaxations, total energies, and charge densities, and the number is increased up to 50 in order to plot the electronic bands. In addition, the studied wires are in the ferromagnetic configuration of Mn spins, because for the three crystal phases shown here the antiferromagnetic configuration is always less stable.

3 RESULTS

3.1 Distortions and cohesive energies: Change in the order of bulk phases

Firstly, we describe zinc-blende nanowires under stretching or compression using different c/a ratios. Our output zinc-blende nanowires are shown in Fig. 1(a). During relaxation, the Mn-As bonds stretch from 2.46 Å to $2.49-2.61$ Å, and the axis length of the wire expands by 12%. The shape of the cross section also changes from a circle to a rhombus. This output shape justifies the more detailed analysis of zinc-blende wires reported below. The input and output hexagonal structures are plotted in Fig. 1(b) with the $\langle 0001 \rangle$ axis being parallel to the axis of the wire (c-plane orientation). We chose cross sections that terminate with As at the edges because these are more stable than those that terminate with Mn.[40] During relaxation, the lengths of Mn-As bonds increase from 2.57 Å to $2.64-2.77$ Å. This large strain ($3-8\%$) compares well with the lattice mismatches measured at the MnAs/GaAs interface ($< 30\%$[41]). Due to the strain associated with relaxation, the hexagonal wires expand along the axis by 15%. The 8-index phase is obtained by the structural relaxation of a compressed zinc-blende wire along the axis with a low c/a ratio ($c/a < 0.9$). This output geometry is drawn in Fig. 1(c), together with its bulk-like zinc-blende counterpart. In the relaxed wires, the Mn-As bonds range in length from 2.68 Å

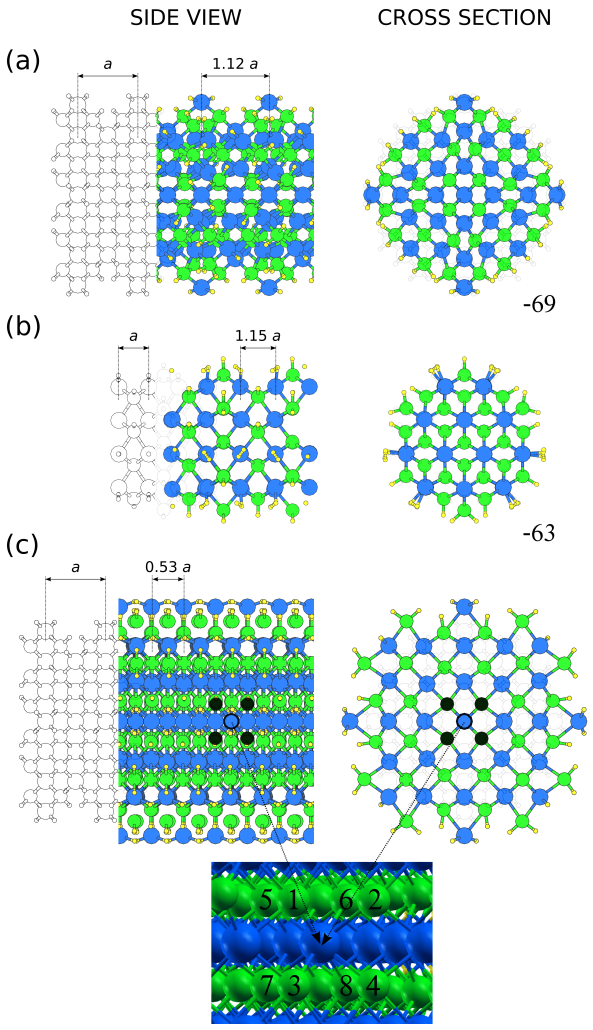

Fig. 1 (Color online) Side and cross-sectional views of polymorphic MnAs nanowires with (a) cubic zinc-blende, (b) hexagonal NiAs-type, and (c) our new crystal symmetry, "8-index". The Mn and As atoms are drawn as large spheres in dark and light grey (blue and green), respectively; and pseudohydrogen atoms with small circles (yellow). The nanowires are plotted at the same scale. The given inset zooms into a central Mn atom and its eight surrounding As first neighbors, as labeled with numbers. For comparison, the stable crystal phases are depicted as in the bulk by empty spheres. The differences in cohesive energies per atom between the wires and the 8-index phase are shown in meV below the cubic and hexagonal geometries. The differences reveal that although the hexagonal wires were more stable than zinc-blende ones, these two phases are almost degenerate.

to 3.13 Å. Compared with the bulk-like zinc-blende structure, the 8-index phase is contracted along the axis down to $0.53a$. These relaxed wires are characterized by eight nearest neighbors around the Mn atoms in the axis. For the As and Mn atoms that lie off-center, the coordination index is either 5 or 6, depending on their positions.

The cohesive energy per atom in the unit cell is defined as $-(E_0 - \sum_{i=1}^{N} E_{\rm at}^i)/N$, where E_0 is the total energy and $E_{\rm at}^i$ is the energy of the i-th free atom. The values obtained are 2.698, 2.635, and 2.629 eV for the 8-index, hexagonal, and cubic phases, respectively. The MnAs nanowires are therefore more stable with the new crystal geometry than with either the hexagonal or zinc-blende one, in this order. The fact that a new phase that differs from the bulk hexagonal is more stable shows the important role of strain in one-dimensional semiconductors. Considering "heat of formation" respect to Mn and As, bulk does not change the 8-index as most stable structure. Previous energy order is proper to the 1-2 nm range because our wires have these diameters. In an intermediate range, this energetic order would change and the one found in bulk would be recovered by increasing the wire diameter.

3.2 Strain fields and winding numbers: Presence of dislocations

We then investigate further the nature of polymorphism in MnAs nanowires by looking at their strain fields and the associated winding numbers.[42] The structural relaxation of the nanowires determine the strain vectors that form the strain fields in their cross sections. We focus on the 8-index and zinc-blende nanowires, as shown in Fig. 2. The strain field that corresponds to the ground state among tried structures shows a homogeneous expansion that can be explained in terms of the compressed input geometry. However, the expansion for the zinc-blende phase is clearly inhomogeneous and must be analyzed in greater detail.

We next investigate these strain fields using homotopy theory.[27] This theory provides the formal basis for the precise description of a large variety of ordered systems by means of a vectorial function. For strain fields, the values of this function are the strain vectors that lie on circumferences centered on the axis of the nanowire. Here, the vectorial function is not continuous but is discretized at each atom. When viewed counterclockwise at these strain vectors, the number of times that they rotate is known as the winding number of the strain field. This number is positive (negative) for counterclockwise (clockwise) rotations. For 8-index, cubic, and hexagonal geometries, the winding numbers are 1, -3, and -5, respectively. Using homotopy theory we know that crystal structures that have distinct winding numbers are not homotopic, i.e., they cannot be *continuously* deformed into one another. Because 8-index and cubic structures are not homotopic, the phase tran-

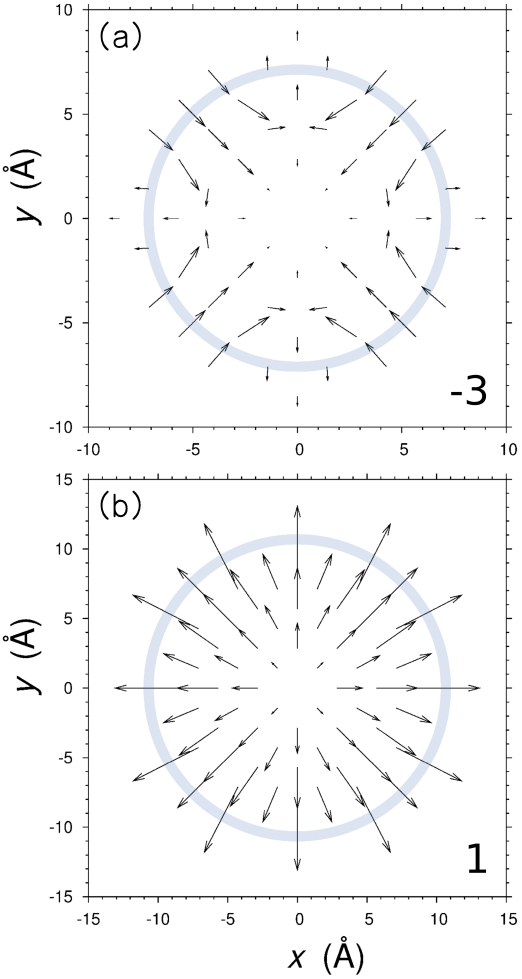

Fig. 2 (Color online) Strain fields in the cross sections of (a) cubic and (b) 8-index nanowires. The strain vectors have been multiplied by 2 for clarity. The numbers in the lower right-hand corners are the winding numbers around the nanowire surfaces. They show the number of times that the strain vectors rotate on the marked circumferences, when viewed counterclockwise. Counterclockwise (clockwise) rotations give positive (negative) winding numbers. The different winding numbers suggest the presence of either dislocations of twins in the zinc-blende wires.

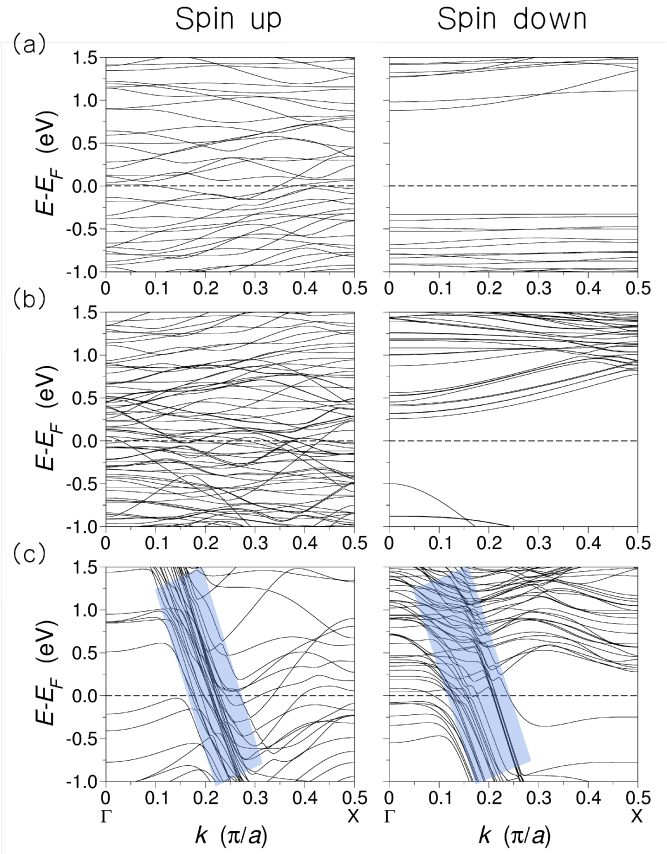

Fig. 3 (Color online) Spin-polarized electronic bands calculated for (a) cubic, (b) hexagonal, and (c) 8-index MnAs nanowires. The shaded areas indicate the slopes for the 8-index bands crossing the Fermi level. Note that the velocities of carriers are thus larger for 8-index wires than for hexagonal or cubic ones.

sition between them suggests the formation of dislocations, such as twins, in the zinc-blende wires.

3.3 Magnetism

We now turn our attention to the ferromagnetism of MnAs nanowires in more detail. The computed total magnetic moments per Mn atom are $4.00\mu_B$, $4.38\mu_B$, and $4.59\mu_B$ in the cubic, hexagonal, and 8-index nanowires, respectively. For comparative purposes, we also calculate the total magnetic moments in the bulk, obtaining values of $4.00\mu_B$ for zinc-blende MnAs and $\sim 3.89\mu_B$ for hexagonal MnAs. This latter value is in good agreement with other calculations,[19] and close to the experimental one for the hexagonal phase, $\sim 3.4\mu_B$.[23,43,44] The former is not compared because we remember that bulk zinc-blende MnAs itself is unstable. The previous magnetic moments $4.00\mu_B$ and $\sim 3.89\mu_B$ show the same decreasing trend as the values of $3.75\mu_B$ and $3.09\mu_B$ reported for bulk MnAs

with zinc-blende and hexagonal structures,[45] respectively. In comparison with previous structural differences in the magnetic moments, the dependence on Mn position is smaller, of the order of $0.1\mu_B$, and may be neglected.

The calculated total magnetic moment of $4.00\mu_B$ per Mn atom in the zinc-blende nanowires can be explained in terms of (i) the large charge transfer of almost three electrons from the Mn cations to their neighboring As anions,[46] and (ii) the strong p(As)$-d$(Mn) hybridization.[47] These two effects are in turn strongly dependent on the Mn-As bond length of $\sim$2.55 Å in the zinc-blende nanowire, which is approximately 2.46 Å as in the zinc-blende bulk.[48] In terms of coordination numbers, the total magnetic moment in the hexagonal phase should be smaller than that in the zinc-blende structure. However, the previous value of $4.38\mu_B$ for the hexagonal wires is larger than $4.00\mu_B$ for the zinc-blende ones and also larger than $\sim 3.89\mu_B$ for the hexagonal bulk. Both the charge transfer from the Mn atoms and the $p-d$ hybridization are reduced because of the longer Mn-As bond length of $\sim$2.70 Å. Similarly, the total magnetic moment of $4.59\mu_B$ for the 8-index phase is related to the even longer Mn-As bond length of $\sim$2.90 Å.

3.4 Electronic bands and spatial distributions of carriers

We finally focus our attention on the electronic properties. The calculated electronic bands are plotted in Fig. 3 as a function of the electron wave vector along the crystal direction, between points Γ and X. In the $E(k)$ curves, it may be seen that the hexagonal and zinc-blende nanowires behave as half-metals due to a gap in the spin-down channel, and that the 8-index ones behave as metals. We note that zinc-blende MnAs is also half-metallic in thin films.[26] From the slope of the dispersion curves we can also estimate the velocities of the carriers close to the Fermi energy. The largest slopes for both spin components occur for the 8-index phase, as shown in the shaded parts of Fig.3(c), arising from a larger atomic compression in the crystal direction. The carrier velocities are thus high for this new structure, higher than they are for the hexagonal and cubic ones. We can change the polytypism and twin planes inside the nanowires by tuning the crystal geometry by strain. This level of control could lead to different transport properties and novel electronic behaviors, like that recently found in semiconductor wires.[49,50]

4 Conclusions

In summary, we investigated the nature of polymorphism in ferromagnetic nanowires of shape memory MnAs using density functional theory. We focused on MnAs as a prototype material with major advantages as compared with nonmagnetic shape memory alloys, related to the electronic and magnetic behaviors dependent on the confinement-induced crystal phase. The experimental structures of the bulk MnAs, quantum dots, and thin films are of the hexagonal NiAs and zinc-blende type. However, the MnAs nanowires are more stable in the so-called '8-index' phase induced by strain in one dimension. The 8-index geometry has been further investigated by comparing its strain field with that of the zinc-blende wires. The strain fields are formed by the strain vectors that arise from the structural relaxation of the atomic positions. Using homotopy theory,[27] we obtained the strain vectors, in a counterclockwise sense, that lay on the outermost circumferences centered on the wires, and counted the number of times that these vectors rotated. For a strain field, this number is its associated winding number. The fact that 8-index and zinc-blende wires have distinctly different winding numbers suggests the formation in the latter of either twins or stacking faults. Moreover, the calculated electronic bands show that the zinc-blende and hexagonal phases are half-metallic, while the most stable strain-induced crystalline structure is metallic and also has high carrier velocities. Our findings thus explain the threefold polymorphism of MnAs nanowires, their electronic and magnetic properties, and broaden the applicability of shape memory MnAs in nanomagnetism and spin-based nanoelectronics. Although it is not our expertise, we could made a suggestion based on our results to look experimentally for the 8-index structure. Similarly to experiments,[12,17] narrow wires can be grown and then apply some compression that could drive to the 8-index structure. Zinc-blende or hexagonal nanowires may contain twins that could be analyzed, for instance, with high resolution trasnmission electron microscopy (HRTEM).

Acknowledgement. This study was supported by funding from the Basque Government through the NANOMATERIALS project (Grant No. IE05-151) under the ETORTEK Program (iNanogune), the Spanish Ministerio de Ciencia y Tecnologia of Spain (Grant Nos. TEC2007-68065-C03-03 and Fis2007-66711-C02-02, and MONACEM projects), and the University of the Basque Country (Grant No. IT-366-07).

References

1 A. M. Morales and C. M. Lieber, *Science*, 1998, **279**, 208.
2 J. D. Holmes, K. P. Johnston, R. C. Doty and B. A. Korgel, *Science*, 2000, **287**, 1471.
3 M. H. Huang, S. Mao, H. Feick, H. Yan, Y. Wu, H. Kind, E. Weber, R. Russo and P. Yang, *Science*, 2001, **292**, 1897.
4 Y. Xia, P. Yang, Y. Sun, Y. Wu, B. Mayers, B. Gates, Y. Yin, F. Kim and H. Yan, *Adv. Mater.*, 2003, **15**, 353.
5 H. Yu, J. Li, R. A. Loomis, L. W. Wang and W. E. Buhro, *Nature Mat.*, 2003, **2**, 517.
6 Y. Cui, L. J. Lauhon, M. S. Gudiksen, J. Wang and C. M. Lieber, *Appl. Phys. Lett.*, 2001, **78**, 2214.
7 C. J. Barrelet, Y. Wu, D. C. Bell and C. M. Lieber, *J. Am. Chem. Soc.*, 2003, **125**, 11498.
8 Y. Huang, X. Duan, Y. Cui and C. M. Lieber, *Nano Lett.*, 2002, **2**, 101.
9 T. M. Whitney, J. S. Jiang, P. C. Searson and C. L. Chien, *Science*, 1993, **261**, 1316.

10 T. Thurn-Albrecht, J. Schotter, G. A. Kastle, N. Emley, T. Shibauchi, L. Krusin-Elbaum, K. Guarini, C. T. Black, M. T. Tuominen and T. P. Russell, *Science*, 2000, **290**, 2126.

11 T. G. Sorop, C. Untiedt, F. Luis, M. Kroll, M. Rasa and L. J. de Jongh, *Phys. Rev. B*, 2003, **67**, 014402.

12 D. Toyli, *J. Young Investigators*, 2008, **16**, year.

13 J. L. Simonds, *Phys. Today*, 1995, **48**, 26.

14 J. Sadowski, P. Dluzewski, S. Kret, E. Janik, E. Lusakowska, J. Kanski, A. Presz, F. Terki, S. Charar and D. Tang, *Nano Lett.*, 2007, **7**, 2724.

15 D. G. Ramlan, S. J. May, J.-G. Zheng, J. E. Allen, B. W. Wessels and L. L. J., *Nano Lett.*, 2006, **6**, 50.

16 M. Hilse, Y. Takagaki, J. Herfort, M. Ramsteiner, C. Herrmann, S. Breuer, L. Geelhaar and H. Riechert, *Appl. Phys. Lett.*, 2009, **95**, 133126.

17 R. Engel-Herbert, T. Hesjedal, J. Mohanty, D. M. Schaadt and P. K. H., *Phys. Rev. B*, 2006, **73**, 104441.

18 M. Tanaka, *Semi. Sci. Technol.*, 2002, **17**, 327.

19 I. Rungger and S. Sanvito, *Phys. Rev. B*, 2006, **74**, 024429.

20 M. C. Newton, S. T. Leake, R. Harder and I. K. Robinson, *Nat. Mat.*, 2010, **9**, 120.

21 R. C. O'Handley, *Modern Magnetic Materials: Principles and Applications*, John Wiley & sons, New York, 2000.

22 J. San Juan, M. L. Nó and C. A. Schuh, *Nature Nanotech.*, 2009, **4**, 415.

23 C. P. Bean and D. S. Rodbell, *Phys. Rev.*, 1962, **126**, 104.

24 M. K. Niranjan, B. R. Sahu and L. Kleinman, *Phys. Rev. B*, 2004, **70**, 180406.

25 K. Ono, J. Okabayashi, M. Mizuguchi, M. Oshima, A. Fujimori and H. Akinaga, *J. Appl. Phys.*, 2002, **91**, 8088.

26 T. W. K. H. S. L. J. Y. L. T. W. Kim, H. C. Jeon and S. Jin, *Appl. Phys. Lett.*, 2006, **88**, 021915.

27 N. D. Mermin, *Rev. Modern Phys.*, 1979, **51**, 591.

28 J. Li and L. W. Wang, *Phys. Rev. B*, 2005, **72**, 125325.

29 G. Kresse and D. Joubert, *Phys. Rev. B*, 1999, **59**, 1758.

30 G. Kresse and J. Furthmüller, *VASP the Guide*, 1999.

31 J. P. Perdew, K. Burke and M. Ernzerhof, *Phys. Rev. Lett.*, 1996, **77**, 3865.

32 J. H. Park, S. K. Kwon and B. I. Min, *Physica B*, 2000, **281&282**, 703.

33 A. B. Shick, J. Kudrnovsky and V. Drchal, *Phys. Rev. B*, 2004, **69**, 125207.

34 M. Galicka, R. Buczko and P. Kacman, *Na*, 2011, **11**, 3319.

35 J. A. Chan, J. Z. Liu, H. Raebiger, S. Lany and A. Zunger, *Phys. Rev. B*, 2008, **78**, 184109.

36 A. Barbier, A. Stierle, N. Kasper, M. Guittet and J. Jupille, *Phys. Rev. B*, 2007, **75**, 233406.

37 C. Echeverría-Arrondo, J. Pérez-Conde and A. Ayuela, *Appl. Phys. Lett.*, 2009, **95**, 043111.

38 C. Echeverría-Arrondo, J. Pérez-Conde and A. Ayuela, *Phys. Rev. B*, 2009, **79**, 155319.

39 C. Echeverría-Arrondo, J. Pérez-Conde and A. Ayuela, *Phys. Rev. B*, 2010, **82**, 205419.

40 A. Kazempour, S. J. Hashemifar and H. Akbarzadeh, *Phys. Rev. B*, 2009, **79**, 195420.

41 A. Trampert, F. Schippan, L. Daweritz and H. Ploog, *Appl. Phys. Lett.*, 2001, **78**, 2461.

42 *The direct analysis of the geometry in very thin wires should in principle produce the same information on dislocation than winding numbers, as we have no other defects. However, the strain analysis is instead much easier.*

43 J. B. Goodenough and J. A. Kafalas, *Phys. Rev.*, 1967, **157**, 389.

44 N. Menyuk, J. A. Kafalas, K. Dwight and J. B. Goodenough, *Phys. Rev.*, 1969, **177**, 942.

45 A. Continenza, S. Picozzi, W. T. Geng and A. J. Freeman, *Phys. Rev. B*, 2001, **64**, 085204.

46 *We look at the charge around atomic spheres because we are dealing with plane wave basis sets, similarly to Mulliken population analysis for localized basis sets. This charge remains close to three electrons after saturation with pseudohydrogens following Ref. [28].*

47 S. Sanvito and N. A. Hill, *Phys. Rev. B*, 2000, **62**, 15553.

48 Y.-J. Zhao, W. T. Geng, A. J. Freeman and B. Delley, *Phys. Rev. B*, 2002, **65**, 113202.

49 M. S. Gudiksen, L. J. Lauhon, J. Wang, D. C. Smith and C. M. Lieber, *Nature*, 2002, **415**, 617.

50 P. Caroff, K. A. Dick, J. Johansson, M. E. Messing, K. Deppert and L. Samuelson, *Nature Nanotech.*, 2009, **4**, 50.